Physics from solar neutrinos in dark matter direct detection experiments

David G. Cerdeño,[1] Malcolm Fairbairn,[2] Thomas Jubb,[1]
Pedro A. N. Machado,[3,4] Aaron C. Vincent,[1] and Céline Bœhm[1,5]

[1]*Institute for Particle Physics Phenomenology (IPPP),*
Durham University, Durham DH1 3LE, UK
[2]*Physics, King's College London, Strand, London, WC2R 2LS, UK*
[3]*Departamento de Física Teórica, Universidad Autónoma de Madrid, Cantoblanco E-28049 Madrid, Spain*
[4]*Instituto de Física Teórica UAM/CSIC, Calle Nicolás Cabrera 13-15, Cantoblanco E-28049 Madrid, Spain*
[5]*LAPTH, U. de Savoie, CNRS, BP 110, 74941 Annecy-Le-Vieux, France*

The next generation of dark matter direct detection experiments will be sensitive to both coherent neutrino-nucleus and neutrino-electron scattering. This will enable them to explore aspects of solar physics, perform the lowest energy measurement of the weak angle $\sin^2\theta_W$ to date, and probe contributions from new theories with light mediators. In this article, we compute the projected nuclear and electron recoil rates expected in several dark matter direct detection experiments due to solar neutrinos, and use these estimates to quantify errors on future measurements of the neutrino fluxes, weak mixing angle and solar observables, as well as to constrain new physics in the neutrino sector. Our analysis shows that the combined rates of solar neutrino events in second generation experiments (SuperCDMS and LZ) can yield a measurement of the pp flux to 2.5% accuracy via electron recoil, and slightly improve the ^{8}B flux determination. Assuming a low-mass argon phase, projected tonne-scale experiments like DARWIN can reduce the uncertainty on both the pp and boron-8 neutrino fluxes to below 1%. Finally, we use current results from LUX, SuperCDMS and CDMSlite to set bounds on new interactions between neutrinos and electrons or nuclei, and show that future direct detection experiments can be used to set complementary constraints on the parameter space associated with light mediators.

I. INTRODUCTION

Direct detection (DD) experiments are the primary tool in the search for weakly-interacting dark matter. Such detectors are sensitive to nuclear recoil signals in the $\sim 1 - 100$ keV range from the scattering of dark matter particles as they stream through the Earth. These experiments typically consist of dense crystals (such as germanium, silicon, or sodium iodide) or liquid noble gases such as xenon or argon. They are located deep in underground mines, shielded from cosmic rays and cosmogenic radiation. DD experiments thus share many similarities with underground neutrino detectors and, as such, may be used to measure neutrino properties. Moreover, their low recoil energy threshold makes them excellent tools to search for new physics at low scales.

In particular, the next generation (G2) of DD experiments is expected to detect neutrinos from nuclear reactions occurring inside the Sun. Future experiments might detect atmospheric neutrinos induced by the interactions of the cosmic rays with the atmosphere, as well as the diffuse background of neutrinos produced in type II supernovae throughout the history of the Universe.

The coherent scattering of these neutrinos with nuclei in direct detection experiments constitutes a severe limitation to the detection of dark matter, since their recoil energy is expected to be similar. This is referred to as the "neutrino scattering floor" [1–6].

For example, the recoil spectrum of a 6 GeV dark matter particle would be very difficult to distinguish from the ^{8}B solar neutrino flux, though one may be able to discriminate both signals by exploiting their different contributions to annual modulation [7, 8], or by using a combination of complementary targets [9] and directional detectors [10, 11] or detectors with improved energy resolution [12].

The detection of coherent neutrino scattering is interesting in itself as this Standard Model (SM) prediction has never been observed in dedicated neutrino experiments, due to the small cross sections and the very low recoil energy involved. Moreover, any deviation to the SM expectation could indicate the existence of new physics at low energy, while the lack of deviation could help to set constraints on light mediators. This attractive possibility is already an integral part of the science programme of direct detection collaborations, and presumably within reach of the future SuperCDMS SNOLAB phase [13] and LZ [14] experiments.

In this work, we focus on the possibility of characterising the physics of solar neutrinos, and of probing new physics with future dark matter experiments. We quantify the precision with which $\sin^2\theta_W$ can be measured at the lowest possible energy scale to date. This can both confirm a long-standing prediction of the standard model; and help search for or rule out effects of new physics, such as a light dark sector, which could change the running of $\sin^2\theta_W$ at low energies (see e.g. Ref. [15]).

Before turning to our results, we begin by briefly summarizing the basics of solar neutrino physics and neutrino scattering off nuclei and electrons in Sections II and III, respectively. In Section IV,

we explore the reconstruction of solar parameters from the combination of data from various DD experiments. In Section V, we determine the constraints that future DD experiments will be able to place on new physics models with light mediators. For concreteness, we take a simplified effective model approach (below the electroweak scale), and constrain the mediator mass and couplings to electrons, quarks, and neutrinos. Finally, we illustrate our results in the case of a light $U(1)_{B-L}$ gauge boson, showing that current experiments (SuperCDMS, CDMSlite and LUX) can exclude new regions of the parameter space. Our conclusions are presented in Section VI.

II. SOLAR NEUTRINOS

In this section and the next, we review the necessary physics of solar neutrino fluxes and direct detection experiments that are relevant for this study and that go into the production of our results.

A. Neutrino contribution

The dominant contributions to the neutrino flux in the lowest energy range arise from the various nuclear fusion and decay processes occurring in the solar core, associated with the Sun's energy production. The primary fusion process in the Sun is $p+p \rightarrow {}^2\mathrm{H}+e^+ +\nu_e$ and leads to the production of neutrinos in a continuum up to $E_\nu \lesssim 400$ keV. These are referred to as pp neutrinos and are by far the largest contributors to the solar neutrino flux below the MeV scale. Recoils from pp neutrinos scattering on target nuclei are virtually undetectable, since the typical momentum transfer is much lower than the threshold energy of a few keV of current DD experiments. However, the electron recoil energies fit comfortably above the $\sim$ keV threshold.

At higher energies but with lower flux (by around three orders of magnitude) we find the neutrinos produced from the CNO cycles, which we will refer to simply as the CNO neutrinos. Within the same energy range there are the monoenergetic neutrino lines at $E_\nu = 862$ keV and 384 keV from ${}^7\mathrm{Be}$. These energies are typically too low to give rise to a nuclear recoil within the range 1-100 keV that current DD experiments are typically optimised for, and too high to give an electron recoil in the right energy range. Some high-metallicity solar models [16] predict CNO fluxes that are over 50% larger than the expected values in standard solar models. However, these also yield other fluxes that are experimentally excluded, and are in general disagreement with spectroscopic data [17].

Finally the decay of ${}^8\mathrm{B}$ nuclei produced in the pp and pep chains yields the highest energy neutrinos, within the 1-10 MeV range. These are expected to produce nuclear recoils in DD experiments near the $E_R \sim$ keV recoil energy threshold. Even though the ${}^8\mathrm{B}$ neutrino flux is six orders of magnitude lower than the pp flux, the coherent enhancement of the cross section with the atomic number ($\sigma \sim A^2$) significantly boosts the detection rate via nuclear scattering and implies that heavy target DD experiments may be sensitive to this signal.

Fig. 1 shows the individual spectra for the solar neutrino fluxes mentioned above. We also use coloured bands to show the reach of the experiments that we consider in this work. Dark shading shows the neutrino energy range that can be seen via coherent nuclear scattering, while the light shaded areas show the reach of electron recoils. In reality, only the pp spectrum is expected to lead to a visible electron recoil signal: this is due to 1) the fact that pp dominates the flux by four orders of magnitude at low energies; and 2) very high radioactive backgrounds expected at larger electron recoil energies, which will dwarf even the upper edge of the pp spectrum (see e.g. Ref. [18]).

Note that atmospheric neutrinos and neutrinos from the diffuse supernova background could also induce nuclear recoil signatures in DD experiments. However, since they are produced at higher energies and with much lower rates, they should only be within the reach of future multi-ton experiments. We disregard them in the present study.

B. Neutrino physics

In the SM, the coherent scattering of solar neutrinos with nuclei (which takes place through the exchange of a Z boson) typically leads to nuclear recoils below 10 keV. Their detection thus requires low-threshold detectors such as SuperCDMS. On the other hand, neutrino-electron interactions (which occur through the exchange of neutral and charged gauge bosons) give rise to electron recoil signatures of a few tens to hundreds of keV.

As the pp flux was first measured by Borexino using electron recoils [19], many authors have proposed the use of nuclear and electron recoil signatures in DD experiments to probe solar observables, test the validity of SM processes, and probe new physics at low energies.

For example Ref. [20] pointed out that a low-threshold Ge detector could improve the measurement of the ${}^8\mathrm{B}$ flux normalisation to better than 3% and Ref. [18] showed that the observation of pp neutrinos in a third generation Xe detector such as DARWIN [21] could lower the statistical uncertainty on the pp flux to less than 1%; this is an overwhelming improvement over the current 10%
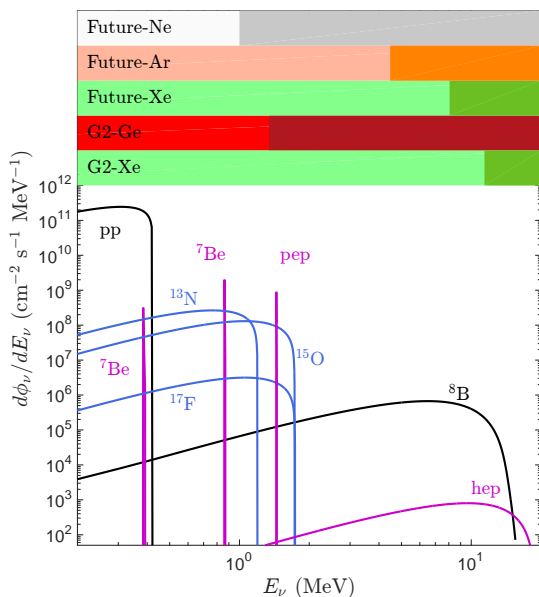
FIG. 1. Spectra of solar neutrinos accessible to direct detection experiments. In black are the *pp* and ^{8}B fluxes that will be seen respectively by electron and nuclear recoils in second generation (G2) and future experiments. CNO fluxes are in blue. The purple Be and pep lines, as well as the subdominant hep flux are not considered in this work. The bands at the top of the figure illustrate the reach of electron recoils (light shading) and nuclear recoils (dark shading) in future experiments, based on the optimistic configurations listed in Table I. A low-threshold experiment with a light target nucleus may be able to probe the CNO fluxes for the first time, provided that backgrounds are low enough and nuclear recoils can be discriminated.

error from Borexino [19]. Such precision measurements can also help distinguish between metal-rich and metal-poor solar models, via the correlation between neutrino production and the environmental abundance of primordial heavy elements [22–25].

The nuclear recoil event rates are sensitive to the weak (or Weinberg) angle θ_W, which expresses the ratio of the charged to neutral weak gauge boson masses,

$$\cos\theta_W \equiv \frac{m_W}{m_Z}, \qquad (1)$$

and effectively determines the ratio between the couplings of the neutrino to the proton versus the neutron at low energies. The quantity $\sin^2\theta_W$ has been determined to very high accuracy at the electroweak scale, in high energy experiments. Given LEP, PETRA and PEP measurements [26, 27], the SM renormalization group equations imply that this parameter should run to $\sin^2\theta_W = 0.2387$ at low energies in the $\overline{MS}$ scheme [28]. Thus far, the lowest-energy direct probe of $\sin^2\theta_W$ has been at scales of 2.4 MeV [29], via atomic parity violation measurements in ^{133}Cs

[30]. Given that the momentum exchange in coherent neutrino-nucleus scattering occurs at energies of a few MeV, and that electron recoils are expected to probe the $\mathcal{O}(10\ \text{keV})$ range, a direct measurement of $\sin^2\theta_W$ in future DD experiments would constitute the first measurement of this quantity in the keV-MeV range.

Finally, precision measurements of solar neutrinos can help constrain new physics contributions, including a sterile component in the solar flux [20], as well as the presence of new mediators, particularly if they are light (below the GeV scale). These light mediators could have important consequences in neutrino physics [31], in the long standing proton radius discrepancy [32], and in light DM scenarios [33]. Indeed, for sufficiently light mediators, the scattering rate will grow as $1/q^2$ as one goes to lower energies, so the low momentum transfer of DD experiments makes them ideal laboratories for such searches.

III. NEUTRINO SCATTERING IN DD EXPERIMENTS

Solar neutrinos might leave a signal in DD experiments, either through their coherent scattering with the target nuclei or through scattering with the atomic electrons.

In general, the number of recoils per unit energy can be written

$$\frac{dR}{dE_R} = \frac{\epsilon}{m_T} \int dE_\nu \frac{d\phi_\nu}{dE_\nu} \frac{d\sigma_\nu}{dE_R}, \qquad (2)$$

where ϵ is the exposure and m_T is the mass of the target electron or nucleus. If several isotopes are present, a weighted average must be performed over their respective abundances.

The SM neutrino-electron scattering cross section is

$$\frac{d\sigma_{\nu e}}{dE_R} = \frac{G_F^2 m_e}{2\pi}\Big[(g_v + g_a)^2 + \qquad (3)$$
$$(g_v - g_a)^2\left(1 - \frac{E_R}{E_\nu}\right)^2 + (g_a^2 - g_v^2)\frac{m_e E_R}{E_\nu^2}\Big],$$

where G_F is the Fermi constant, and

$$g_{v;\mu,\tau} = 2\sin^2\theta_W - \frac{1}{2}; \ g_{a;\mu,\tau} = -\frac{1}{2}, \qquad (4)$$

for muon and tau neutrinos. In the case $\nu_e + e \rightarrow \nu_e + e$, the interference between neutral and charged current interaction leads to a significant enhancement:

$$g_{v;e} = 2\sin^2\theta_W + \frac{1}{2}; \ g_{a;e} = +\frac{1}{2}. \qquad (5)$$

The neutrino-nucleus cross section in the SM reads

$$\frac{d\sigma_{\nu N}}{dE_R} = \frac{G_F^2}{4\pi}Q_v^2 m_N\left(1 - \frac{m_N E_R}{2E_\nu^2}\right)F^2(E_R), \quad (6)$$

3

Experiment	ϵ (ton-year)	$E_{th,n}$ (keV)	$E_{th,o}$ (keV)	E_{max} (keV)	$R(pp)$	$R(^8\text{B})$	$R(\text{CNO})$
G2-Ge	0.25	0.35	0.05	50	−	[62 − 85]	[0 − 3]
G2-Si	0.025	0.35	0.05	50	−	[3 − 3]	0
G2-Xe	25	3.0	2.0	30	[2104 − 2167]	[0 − 64]	0
Future-Xe	200	2.0	1.0	30	[17339 − 17846]	[520 − 10094]	0
Future-Ar	150	2.0	1.0	30	[14232 − 14649]	[6638 − 12354]	0
Future-Ne	10	0.15	0.1	30	[1141 − 1143]	[898 − 910]	[21 − 63]

TABLE I. Physical properties of idealized G2 (top 3 lines) and future experiments used in our forecasts, with the expected total pp and boron-8 neutrino events, based on planned masses of similar experiments and an exposure of 5 years. We give nominal and optimistic threshold energies and maxima for the energy windows based on the energy beyond which backgrounds are expected to dominate. Our idealized G2 Ge and Si experiments are similar to the SuperCDMS SNOLAB phase, while the G2 Xe experiment is similar to LZ projections. Future experiments are similar to the planned DARWIN experiment, or an argon phase of a DARWIN-like experiment.

where $F^2(E_R)$ is the nuclear form factor, for which we have taken the parametrisation given by Helm [34].[1] Q_v parametrises the coherent interaction with protons (Z) and neutrons ($N = A - Z$) in the nucleus:

$$Q_v = N - (1 - 4\sin^2\theta_W)Z. \qquad (7)$$

Current DD experiments excel at the discrimination of nuclear recoils from electron recoils. By design, these detectors are engineered in such a way that the nuclear recoil background induced by either radioactive processes or cosmic-rays is extremely small. Thus, in our analysis we consider the idealised situation in which nuclear recoils are produced solely by coherent neutrino scattering. This assumes that any nuclear recoil backgrounds can be completely identified and eliminated and that either no signal for dark matter has been found or that a potential dark matter background can be discriminated.

On the other hand, electron recoils from radioactive processes are copious, and would constitute a very important background for the study of neutrino-electron scattering. Future advances in the design and construction of extremely radiopure detectors will allow a significant reduction of the noise levels. For example, current rates in Xenon100 electron recoil band are of the order of 3×10^3 events $\text{ton}^{-1}\,\text{yr}^{-1}\,\text{keV}^{-1}$ [36], but projected xenon-based experiments such as DARWIN aim to reduce this to $\mathcal{O}(10)$ events $\text{ton}^{-1}\,\text{yr}^{-1}\,\text{keV}^{-1}$ [18] for recoil energies below 100 keV. In our analysis we will consider the idealized situation in which the electron recoil background is negligible compared to standard $\nu - e$ scattering.

For concreteness, we have specified in Table I several experiment types that are similar in threshold, efficiency and exposure specifications to upcoming experiments. We do not restrict ourselves to experiment-specific parameters such as

————

[1] Since we are mainly probing recoil energy regimes that are lower than typical DM searches, the uncertainty due to the choice of form factor is minimised [35].

background spectrum and resolution since these are difficult to estimate and subject to significant change. We thus include a second-generation germanium and silicon experiment (inspired by SuperCDMS SNOLAB), a second-generation xenon experiment (inspired by LZ), as well as future DARWIN-like xenon and argon experiments. Finally, we include a neon-based experiment to illustrate the possibility of observing the ^{15}O and ^{13}N neutrinos from the CNO cycle with future low-mass TPCs. The very recent Ref. [37] contains some discussion of the pep line; however, even for the most optimistic configuration that we consider, we would see at most 2 pep events, versus a possible ~ 60 CNO neutrinos in the same energy range.

Tab. I shows the parameters that we use for our benchmark models, and the expected number of events from electron recoils of pp neutrinos, $R(pp)$, and nuclear recoils from ^{8}B and CNO neutrinos ($R(^8B)$ and $R(\text{CNO})$, respectively). We have specified an exposure similar to planned experiments, as well as two sets of threshold energies that are respectively nominal and optimistic projections of what could be achieved in such experiments ($E_{th,n}, E_{th,o}$). Last, as a stand-in for realistic efficiency curves, we take the efficiency in each experiment to rise linearly from 50% at the threshold, to 100% at 1 keV (for Ge, Si, Ne) or 5 keV (Xe, Ar).

IV. SOLAR AND STANDARD MODEL PHYSICS

The various components of the standard solar model (SSM) make use of very well-understood physics, but depend on over 20 individual input parameters. These include the solar age, luminosity, radial opacity dependence, diffusion rates, nuclear cross sections and the elemental abundances at age zero.

Since the downward revision of photospheric elemental abundances a decade ago, some tension has remained between predictions of the SSM and independent observations using helioseismology.

In this section, we focus on two parameters, the overall metallicity Z/X and the effective change in opacity with respect to the SSM, $\delta\kappa$. With enough information, one should be able to study the effect of individual elements on the neutrino fluxes. However, with so few observables it is not possible to distinguish them.

We perform a Fisher analysis to extract the predicted sensitivity of future experiments to the various parameters studied here. For each experiment k which measures an observable ϕ^k with error σ_k, the Fisher information matrix is

$$F_{ij}^k = \frac{1}{\sigma_k^2} \frac{\partial \phi^k}{\partial \theta_i} \frac{\partial \phi^k}{\partial \theta_j}, \qquad (8)$$

where the indices i, j run over the parameters $\{\theta\}$ that we wish to constrain. The total fisher matrix is simply $F \equiv \sum_k F^k$. Assuming gaussianity in the parameters of interest, the covariance matrix is

$$C = F^{-1}. \qquad (9)$$

The diagonal elements of C are the forecasted errors on each individual parameter given the experiments included in F, while the off-diagonal components give the linear degeneracies.

For electron scattering described in Eq. 6, the uncertainty on the neutrino mixing angles θ_{12} and θ_{13} lead to an extra source of uncertainty on the measured pp flux. For G2 experiments, we take the 1σ errors on these parameters from the latest NuFit determinations[2] [38, 39], which lead to a 1.15% uncertainty on the inferred neutrino flux from neutrino scattering. We do not include this error for the Future experiments, as projects such as JUNO [40] will constrain these quantities to very high precision[3,4].

A. Neutrino fluxes and $\sin^2\theta_W$

The lowest-energy sensitivity to $\sin^2\theta_W$ arises through neutrino-electron scattering, which probes interactions via momentum transfers of order tens of keV (though nuclear scattering recoil energies are lower, the transferred momentum $q = \sqrt{2E_R m_N}$ is much higher).

If only the experimental measurement by Borexino [19] of the pp flux is considered, then we find that future DD experiments can measure $\sin^2\theta_W$ down to about 20% uncertainty. However,

much greater precision can be attained through the addition of the luminosity constraint on the total neutrino flux from the Sun. Using the global bounds derived in Ref. [41], the resulting 0.6% error on the pp flux allows G2 experiments to narrow down the $\sin^2\theta_W$ measurement to within 4.5%. This is solely due to an LZ-like xenon experiment, as the pp flux will remain inaccessible to solid-state experiments due to high backgrounds. Future liquid noble gas experiments can bring this error down to 1.4%. The projected uncertainties in different configurations are given in Tab. II.

Lowering the threshold has little impact on these numbers, since the electron recoil rate is fairly insensitive to the lower energy. The expected precision on the measurement of $\sin^2\theta_W$ is thus very close to the results of present experiments, with the additional advantage that direct detection experiments can access an energy range that is unreachable in a collider setup, and is two orders of magnitude lower than results from atomic parity violation experiments. As a final remark about $\sin^2\theta_W$, although the precision of future DD experiment would be about 10 times weaker than future experiments like MOLLER [42], the energy scale would be a factor 10,000 smaller. Hence, DD experiments are sensitive to new physics at much lighter scales.

By instead fixing the value of $\sin^2\theta_W$ to the expected value given by running the LEP measurement down to low energies using the $\overline{\text{MS}}$ scheme, $\sin^2\theta_W = 0.2387 \pm 7 \times 10^{-5}$ [26], the neutrino fluxes can be independently measured. One can then predict the precision of the ^{8}B and pp flux measurements from future experiments. The one-dimensional errors on each of these fluxes are presented in the first column of Tab. II. The reduction of error in the pp flux is striking: the G2 xenon experiment will bring this from the current 10% down to 2.2%; future experiments bring this down even further, to 0.6%[5]. Note that lowering the threshold has very little effect on the measured pp flux, as the electronic recoil rate does not rise sharply at lower energies.

In contrast, a lower threshold allows significantly more ^{8}B neutrinos to be measured, this time allowing a SuperCDMS-like germanium experiment to drive the G2 measurements, albeit with only a small improvement ($\pm 1.9\%$) with respect to current measurements ($\pm 2\%$). As a further consequence, the optimistic detector configurations have almost twice the sensitivity as the nominal ones. A xenon phase of DARWIN could thus measure the ^{8}B flux better than even a dedicated future neutrino experiment such as Hyper-Kamiokande [43], for which we show a sensitivity projection based on one year of data taking in the

---

[2] http://www.nu-fit.org

[3] More concretely, JUNO expects to measure $\sin^2\theta_{12}$ to within 0.67%, leading to an error on the event rate in DD experiments of $\sim 0.2\%$.

[4] We also point out that by using independent measurements of the pp flux, one can instead use the DD observations as a constraint on $\sin^2\theta_{12}$.

[5] The small difference with the 1% error quoted in Ref. [18] is due to the larger exposure we take here.

Exp.	$\phi_\nu^{^8\text{B}}$	ϕ_ν^{pp}	$\sin^2\theta_W$
Measured	2.0% [a]	10.6 % [b]	
G2	1.9% (1.9%)	2.5 % (2.5%)	4.6% (4.5%)
Future-Xe	1.8% (0.9%)	0.7% (0.7%)	1.7% (1.7%)
Future-Ar	1.0% (0.6%)	0.6% (0.5%)	1.5% (1.4%)
HyperK[c]	1.43%	–	–

[a] Global fit [44] $\phi_\nu^{^8\text{B}} = (5.1 \pm 0.1) \times 10^6$ cm^{-2} s^{-1}
[b] Borexino [19] measurement $\phi_\nu^{pp} = (6.6 \pm 0.7) \times 10^{10}$ cm^{-2} s^{-1}
[c] Based on 1 year projected data [43]

TABLE II. Current and projected errors on the ^{8}B and pp neutrino fluxes (with fixed $\sin^2\theta_W = 0.2387$), and on $\sin^2\theta_W$ at low energies (using the solar neutrino flux data from SuperK, SNO+ and Borexino, and the luminosity constraint on the pp flux from [41]). The numbers are shown for the nominal (optimistic) thresholds of Tab. I. Each subsequent experiment set includes the previous one measurements.

Exp.	δ_k	Z/X
Solar observations	0.04	0.0024
Including neutrinos	0.034	0.0013
Future-Xe	0.033 (0.033)	0.0013 (0.0013)
Future-Ne	0.032 (0.030)	0.0013 (0.0012)

TABLE III. Current and projected errors on the average opacity (δ_k) and the metallicity (Z/X), using the nominal (optimistic) thresholds of Tab. I. Each subsequent experiment set includes the previous one measurements. Approximate error on $\delta\kappa$ is from helioseismological observations [45]; error on the metallicity comes from the measured solar abundances [48]. The neutrino data used for the second line are the same as Tab. II.

last line of Tab. II.

B. Solar observables and CNO neutrinos

We now turn to the impact of coherent nuclear scattering and electron recoil measurements on solar modelling. An accurate measurement of pp and ^{7}Be neutrino fluxes, together with the luminosity constraint [47], tell us the exact fraction of the solar energy that comes from the pp-chain, and thus indirectly constrains the CNO cycle which makes up the remaining $\sim 1\%$ of energy generation. Such a measurement would therefore constitute the most accurate probe yet of the ^{13}N and ^{15}O neutrino fluxes, which have yet to be experimentally observed.

To illustrate how DD experiments can help infer solar properties, we use the partial derivatives from linear solar models [45, 46] of the neutrino fluxes with respect to an overall shift in opacity $\delta\kappa$ and with respect to the metal-to-hydrogen ratio Z/X.[6] Fig. 2 illustrates the impact of future

————

[6] Strictly speaking, one should correlate all neutrino fluxes

experiments on these observables. Since they are both highly correlated with the ^{8}B flux (and less so to pp), the main effect is to narrow down the degeneracy in the opacity-metallicity space. This indicates that, when combined with new neutrino data, a precise independent measurement of either κ or solar metallicity can pin down the other observable to a high degree of precision, though direct detection experiments on their own are of limited help. In Tab. III, we show the projected errors from DD experiments on the determination of opacity and metallicity.

We finally return to the ^{13}N and ^{15}O neutrino fluxes. These lie approximately an order of magnitude below the ^{7}Be line, although they dominate the solar spectrum at electron recoil energies above ~ 750 keV. In this range, material backgrounds dominate by several orders of magnitude, making discrimination of the CNO neutrinos highly unlikely. One may search for CNO events in the nuclear recoil spectrum. This requires:

1. A light target to reach neutrino energies below the ^{8}B peak;

2. A low threshold (e.g., below 0.25 keV for Ne);

3. Good discrimination between nuclear and electron recoil events.

Light elements such as F, Na, Ne and Al, would give 0.02 to 0.01 ^{15}O events per kg year with a 0.1 keV threshold. Superheated fluids such as C_3F_8 targets are light enough, but current thresholds tend to be far too large [49]. Supercooled scintillating sapphire bolometers such as ROSEBUD [50] can attain a ~ 100 eV threshold. However, their exposures tend to be limited to a few hundred gram-days. An alternative which satisfies 1) and 2) would be pressurized noble gas TPCs. Thresholds of 100 eV can in principle be obtained for Ne with such a setup [51, 52]. The low threshold is key to this observation: increasing E_{th} by only 50% yields a substantial drop in the observable CN flux, from 63 to 21 events for 10 ton-years of neon. Discrimination between nuclear and electron recoils at such low energies is extremely challenging and one might rather rely on the radiopurity of the experiment and the directionality of solar neutrinos. In green, we show the effect of a future neon-based experiment on solar observables in Fig. 2. CNO neutrinos are a direct probe of the abundances of these elements – and thus of the metallicity Z/X which C, N, O dominate. Even a modest measurement of the CNO flux (63 events in our optimistic case) can thus provide a small break in the degenerate parameter space.

————

with individual elemental and with a radially-dependent parametrization of $\delta\kappa(r)$. Given the paucity of observables, however, we restrict ourselves to these more general quantities.
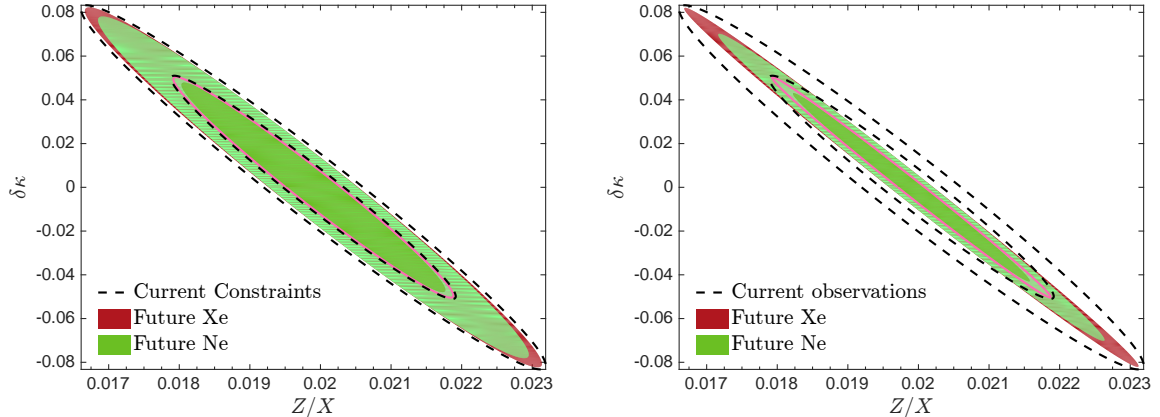
FIG. 2. Estimate of the potential improvement of constraints on the solar metallicity fraction Z/X and the deviation of opacity from the standard solar model $\delta\kappa$, through the use of neutrino measurements. Left: using the nominal thresholds $E_{th,n}$ from Table I; right: using the optimistic threshold energies $E_{th,o}$. The main effect comes from the correlation between $\phi_\nu^{^8\mathrm{B}}$ and these two quantities (although the small effect of pp is also included), based on linear solar models [45, 46]. The addition of these neutrino data are reflected in a narrower correlation line. To break this degeneracy, the neutrino flux from the subdominant CN cycle must be included, since these are the only direct probe of the light elements which contribute directly to Z/X.

V. CONSTRAINTS ON NEW PHYSICS

The simultaneous measurement of the neutrino-electron and neutrino-nucleus couplings enables us to test the predictions for models of new physics in two complementary directions.

A. Simplified models

To parametrise new physics at a very low scale, we write the Lagrangian for energies below electroweak symmetry breaking which incorporates scalar and vector mediators that couple to neutrinos, electrons, and quarks in a model independent way. The additional terms in the low energy Lagrangian are shown in the second column of Table IV, for a scalar (or pseudoscalar) mediator ϕ, and vector (or axial vector) mediator Z'. The resulting neutrino-nucleus and neutrino-electron scattering cross sections are shown in the third and fourth columns. We neglect terms of order $E_R/E_\nu \lesssim 10^{-2}$ and, in the case of pseudoscalar interactions, couplings to heavy quarks.

In our model, we introduce couplings to quarks, but in order to correctly describe scattering with nuclei, the couplings of the mediator to the nucleons are needed. This is done by calculating the matrix element of the quark Lagrangian with nucleon states, which leads to the following changes

at the Lagrangian level:

$$c_q \bar{q}q \rightarrow f_{Tq}^{(\mathcal{N})} \frac{m_\mathcal{N}}{m_q} \bar{\mathcal{N}}\mathcal{N}, \tag{10}$$

$$c_q \bar{q}i\gamma^5 q \rightarrow c_A^\mathcal{N} \bar{\mathcal{N}}i\gamma^5\mathcal{N}, \tag{11}$$

$$c_q \bar{q}\gamma^\mu\gamma^5 q \rightarrow \Delta_q^{(\mathcal{N})} \bar{\mathcal{N}}\gamma^\mu\gamma^5\mathcal{N}, \tag{12}$$

$$c_q \bar{q}\gamma^\mu q \rightarrow c_V^\mathcal{N} \bar{\mathcal{N}}\gamma^\mu\mathcal{N}, \tag{13}$$

where $\mathcal{N}$ is the nucleon (proton or neutron) spinor, and the coefficients are given numerically in Ref. [53] (see also Ref. [54] and references therein, as well as Refs. [55, 56] for more recent determinations of the pion-sigma term and of the strangeness content of the nucleon based on experimental and EFT results, which enter into these coefficients). More specifically, in our framework where the couplings to all quarks are the same, the coherence factors, Q, of the cross sections induced by these different interactions (see Table IV) are

$$\frac{Q'_s}{g_{\nu,\phi}g_{q,s}} = \sum_{\mathcal{N},q} \frac{m_\mathcal{N}}{m_q} f_{Tq}^{(\mathcal{N})} \approx 14A + 1.1Z, \tag{14}$$

$$\frac{Q'_v}{g_{\nu,Z'}g_{q,v}} = 3A, \tag{15}$$

$$\frac{Q'_a}{g_{\nu,Z'}g_{q,a}} = S_N \sum_q \Delta_q^{(p)} \approx 0.3S_N, \tag{16}$$

$$Q_v = N - (1 - 4\sin^2\theta_W)Z, \tag{17}$$

$$Q_a = S_N(\Delta_u^{(p)} - \Delta_d^{(p)} - \Delta_s^{(p)}) \approx 1.3S_N. \tag{18}$$

The primed coherence factors refer to new interactions. Although the axial vector interaction at low energies is also coherent, it couples to the spin operator, so the coherence factor is proportional to the nuclear spin $S_N^2 \sim \mathcal{O}(1 - 10)$, rather than $A^2 \sim 10^4$. This assumes a simple shell model,

Mediator	$\mathcal{L}$	$d\sigma_e/dE_R - d\sigma_e^{\rm SM}/dE_R$	$d\sigma_N/dE_R - d\sigma_N^{\rm SM}/dE_R$
Scalar	$(g_{\nu,\phi}\phi\bar\nu_R\nu_L + h.c.)$ $+ \phi\bar\ell g_{\ell,s}\ell + \phi\bar q g_{q,s}q$	$\dfrac{g_{\nu,\phi}^2 g_{e,s}^2 E_R m_e^2}{4\pi E_\nu^2\left(2E_R m_e + m_\phi^2\right)^2}$	$\dfrac{Q_s'^2 m_N^2 E_R}{2\pi E_\nu^2\left(2E_R m_N + m_\phi^2\right)^2}$
Pseudoscalar	$(g_{\nu,\phi}\phi\bar\nu_R\nu_L + h.c.)$ $- i\gamma^5\phi\bar\ell g_{\ell,p}\ell - i\gamma^5\phi\bar q g_{q,p}q$	$\dfrac{g_{\nu,\phi}^2 g_{e,p}^2 E_R^2 m_e}{8\pi E_\nu^2\left(2E_R m_e + m_\phi^2\right)^2}$	0
Vector	$g_{\nu,Z'} Z'_\mu \bar\nu_L \gamma^\mu \nu_L$ $+ Z'_\mu \bar\ell\gamma^\mu g_{\ell,v}\ell + Z'_\mu \bar q \gamma^\mu g_{q,v} q$	$\dfrac{2\sqrt2 G_F m_e g_v g_{\nu,Z'} g_{e,v}}{\pi\left(2E_R m_e + m_{Z'}^2\right)}$ $+ \dfrac{m_e g_{\nu,Z'}^2 g_{e,v}^2}{2\pi\left(2E_R m_e + m_{Z'}^2\right)^2}$	$-\dfrac{G_F m_N Q_v Q_v'(2E_\nu^2 - E_R m_N)}{2\sqrt2 E_\nu^2\left(2E_R m_N + m_{Z'}^2\right)}$ $+ \dfrac{Q_v'^2 m_N(2E_\nu^2 - E_R m_N)}{4\pi E_\nu^2\left(2E_R m_N + m_{Z'}^2\right)^2}$
Axial Vector	$g_{\nu,Z'} Z'_\mu \bar\nu_L \gamma^\mu \nu_L$ $- Z'_\mu \bar\ell \gamma^\mu g_{\ell,a}\gamma^5\ell$ $- Z'_\mu \bar q \gamma^\mu g_{q,a}\gamma^5 q$	$\dfrac{2\sqrt2 G_F m_e g_a g_{e,a} g_{\nu,Z'}}{\pi\left(2E_R m_e + m_{Z'}^2\right)}$ $+ \dfrac{m_e g_{\nu,Z'}^2 g_{e,a}^2}{2\pi\left(2E_R m_e + m_{Z'}^2\right)^2}$	$\dfrac{G_F m_N Q_a Q_a'(2E_\nu^2 + m_N E_R)}{2\sqrt2\pi E_\nu^2\left(2E_R m_N + m_{Z'}^2\right)}$ $- \dfrac{G_F m_N Q_v Q_v' E_\nu E_R}{\sqrt2\pi E_\nu^2\left(2E_R m_N + m_{Z'}^2\right)}$ $+ \dfrac{Q_a'^2 m_N(2E_\nu^2 + E_R m_N)}{4\pi E_\nu^2\left(2E_R m_N + m_{Z'}^2\right)^2}$

TABLE IV. New Lagrangian terms and differential cross sections with the nucleus N and electron e for the four types of new mediator we consider. Note the negative interference in the vector and axial case with the SM contribution. The couplings g_v and g_a are defined in Eq. (4). The coherence factors Q_i are defined in Eqs. (14-18).

whereby any unpaired nucleon contains the full J quantum number of the nucleus in its ground state.

We assume that the mediators are light (below the few GeV scale) and their couplings to SM particles are small. Therefore, their contribution to electron and nucleus scattering (via t-channel exchange) should be negligible at a high momentum transfer $q^2 \gg m_{\phi,Z'}^2$ but will be enhanced for low scale measurements.

B. Predicted event rates and sensitivities

In Fig. 3 we show the effect that the presence of scalar, vector and axial vector interactions would have upon the rate of scattering events per ton-year as a function of the low-energy threshold. The rate of electron recoil events for a ^{132}Xe target, as well as coherent nuclear recoil events for a variety of different target materials and mediator masses are plotted. In all cases shown, the new physics contribution grows with lower recoil energies, showing the need for low-threshold detectors.

Electron recoil spectra (shown on the left column) are from pp neutrinos, the lowest energy and most copious neutrinos produced in the Sun. Since lowering the threshold of detection does not open up any new sources of neutrinos, a threshold of $E_{th} \sim 1$ keV is sufficient to maximize the SM event rate. The size of the new-physics contribution is dictated by the mass of the mediator and the corresponding coupling. In the limit of small mediator masses, the differential cross section in Tab. IV scales as $d\sigma/dE_R \propto E_R^{-1}$ for scalar mediators and $d\sigma/dE_R \propto E_R^{-2}$ for vector and axial vector mediators, thus leading to substantial changes at low energies. Therefore, if the experimental threshold is low enough, an enhancement of the signal with respect to the SM prediction could be observed. This does not hold for pseudoscalar mediators, as shown in Fig. 5, since in the small mass limit $d\sigma/dE_R$ is energy-independent. Although we are only showing the results for ^{132}Xe, the rates for any other target can be found by rescaling by the corresponding number of electrons per unit mass.

For nuclear recoils the integrated event rate also increases sharply with decreasing threshold. This can be seen as a sharp break in the right-hand panels of Fig. 3. This break corresponds to the intersection of new physics and SM contributions and its location depends on the values of the couplings. The fact that this enhancement becomes visible in these figures around the same energy as the CNO flux is a coincidence due to the choice of coupling, but the CNO contribution nonetheless results in further enhancement.

The target material dependence is very pronounced due to kinematics, as the maximum recoil energy is suppressed by the large nucleus mass,

$$E_{R,\max} = \frac{2E_\nu^2}{(m_N + 2E_\nu)} \, , \qquad (19)$$

For this reason, heavier targets need a lower threshold to probe both new fluxes of neutrinos and new physics processes at low energies. For example, whereas $E_{th} \approx 2$ keV is needed for xenon to be sensitive to ^{8}B neutrinos, these can be accessed by a hypothetical detector based on neon with only $E_{th} \approx 10$ keV. The material dependence also enters into the coherence factors (Eqs. 14–18) for nuclear recoils which in turn depend on A/Z.

As in the case of electron recoils, the most pronounced deviations from the SM prediction occur

in the limit where the mediator mass is small. Indeed, in such a case, the differential cross section scales as $d\sigma/dE_R \propto E_R^{-1}$ for scalar mediators and $d\sigma/dE_R \propto E_R^{-2}$ for vector and axial vector mediators when the new physics contributions dominate. Once more, this leads to an enhancement of the cross section for low recoil energies. We do not show the nuclear recoil rates expected for a pseudoscalar mediator, since the nuclear form factor cancels out when the couplings to all light quarks are identical [53].

As an additional remark on the axial vector and vector mediator cases, the interference between the standard Z and Z' amplitudes become important when these are comparable in magnitude. Remarkably, this interference is destructive due to the chiral structure of the Z couplings, which may lead to an overall suppression of events with respect to the SM prediction. We have illustrated this possibility in Fig. 3 for the case of vector couplings.

The projected constraints on light scale physics are shown in Figs. 4 and 5, for different mediators and target materials. The bands enclose the nominal and optimistic scenarios defined in Tab. I. They are wider for nuclear recoils (right panels) in comparison to electron recoils (left panels) since the dependence with the threshold energy is more pronounced. Depending on the mediator mass, electron recoils could probe couplings below 10^{-6}, while the bounds from nuclear recoils would range from 10^{-3} to 10^{-6}. In the case of a vector mediator scattering off nuclei (middle right plot), the destructive interference with the SM Z contribution may lead to disconnected regions, e.g., for a G2 silicon-based detector. It is worth remembering at this point that we are basing our projections on the assumption that backgrounds can be removed. As discussed above, this is a reasonable hypothesis for the case of nuclear recoils but more challenging for electron recoils.

C. Bounds for a $U(1)_{B-L}$ model

To put the sensitivity of future DD experiments in context, we illustrate our results with the specific example of a light $U(1)_{B-L}$ gauge boson, a construction that was studied in Ref. [57] for $\nu - e$ scattering. In this case, a new vector mediator couples to the $B-L$ quantum numbers of standard model particles. Quarks therefore carry charge $1/3$ under this new gauge coupling, while leptons have charge -1.

In Fig. 6 we present our bounds as before. The coloured lines are the result of this study. We use the optimistic threshold scenarios of a G2 germanium (red lines) and xenon experiment (blue), as well as for a future DARWIN-like xenon target (green). We separate the limits that can be inferred from nuclear (solid lines) and electron re-

coils (dashed). As in the cases shown in Fig. 4, electron bounds tend to do better, thanks to the larger pp flux and to the closer kinematic matching between the solar neutrino energies and electron mass, allowing for higher recoil energies.

Our results in Fig. 6 are overlaid on excluded areas from previous studies, in the plane of gauge coupling g_{B-L} versus mediator mass. A detailed description of each bound can be found in Ref. [57] and references therein (see also Ref. [58] for the TEXONO and CHARM-II limits). It should be emphasized that these limits are not model-independent, as they are sensitive to the coupling between the gauge boson and a specific fermion, as well as to the Lorentz structure of the coupling. These bounds fall into three broad categories:

- **Coupling to electrons (or muons) only**
  "Atomic physics" (measurements of energy levels of atomic excited states), "Sun" and "Globular Clusters" (star cooling via the emission of the mediator), "Borexino" (solar neutrinos scattering off electrons), "TEXONO" and "GEMMA" (reactor neutrinos scattering off electrons), as well as CHARM-II (accelerator neutrinos scattering off electrons) all require a coupling to electrons. The region labeled as "Z' capture in Sun" is not well understood: although the Sun would not lose energy due to Z' emission, solar dynamics could be severely modified, and exact bounds have yet to be computed. The anomalous magnetic moment bounds require couplings to electrons or muons. Moreover, these curves only apply to pure vector couplings (e.g., the curve for axial vector couplings does not flatten at low mediator masses [60, 61]).

- **Coupling to electrons and/or quarks**
  "Fixed target" bounds require coupling to electrons only or both electrons and light quarks, depending if the experiment considered is an electron or proton beam dump. For the first, the mediator is produced by radiation when e^- collide with a target, while in proton dump experiments, the production is dominated by pseudoscalar meson decays (e.g. $\pi^0 \to \gamma Z'$). For both cases, the signature consists of Z' decay to $e^+ e^-$ (the sharp cut on the left of this region corresponds to $2\,m_e$, below which the production of two electrons is kinematically forbidden). Notice that a larger coupling to neutrinos would enhance the mediator invisible branching ratio, weakening this bound. The "Fixed Target" region shown in Fig. 6 includes only electron dump experiments. Proton dump experiments are almost entirely within that region and their inclusion will not change our conclusions. The "B-factories" region requires non
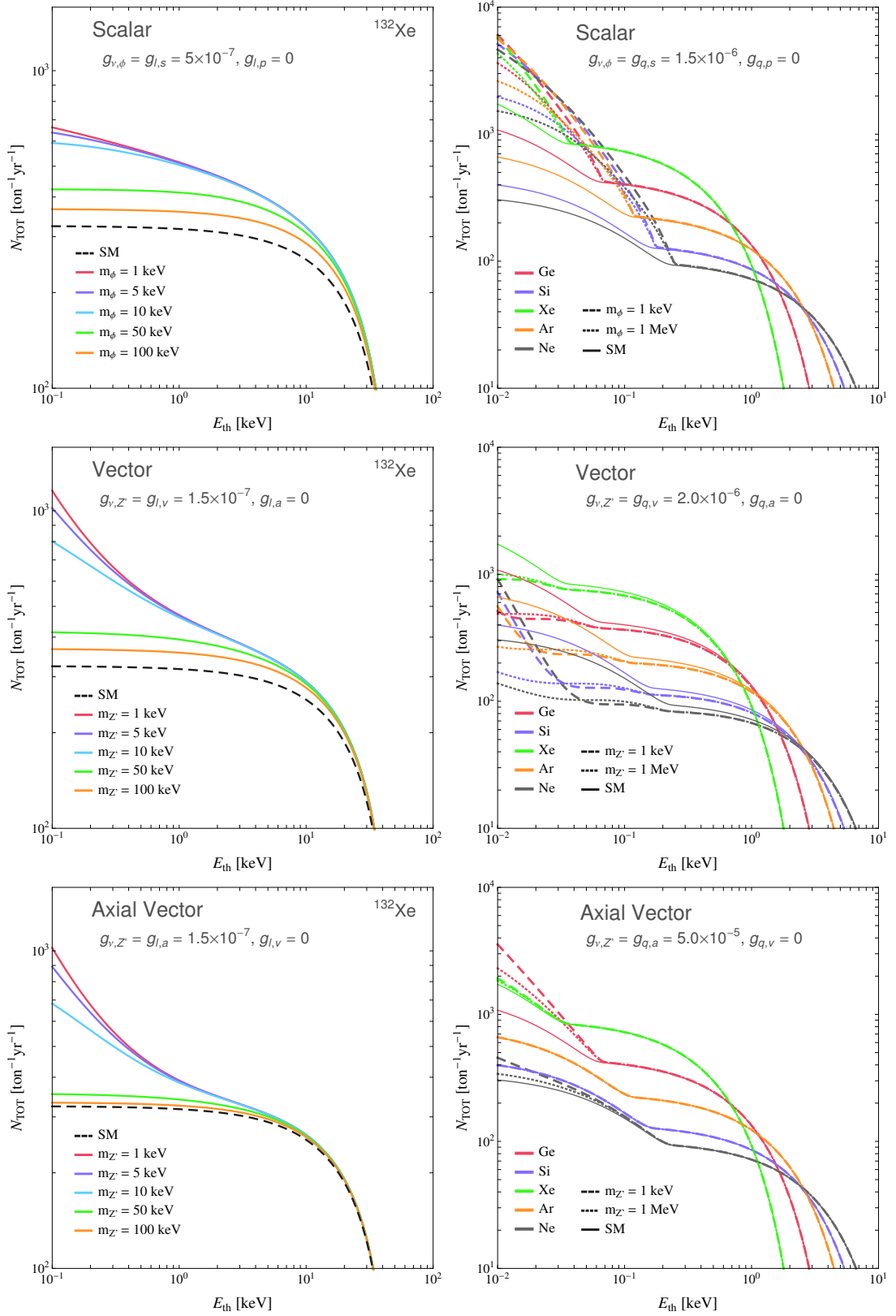
FIG. 3. Electron recoil (left) and nuclear recoil (right) integrated rates as a function of the experimental threshold energy E_{th}. Electron recoils are normalised to ^{132}Xe while nuclear recoils are plotted for a variety of target materials. Top: scalar coupling; middle row: vector coupling; lower panels: axial vector coupling.
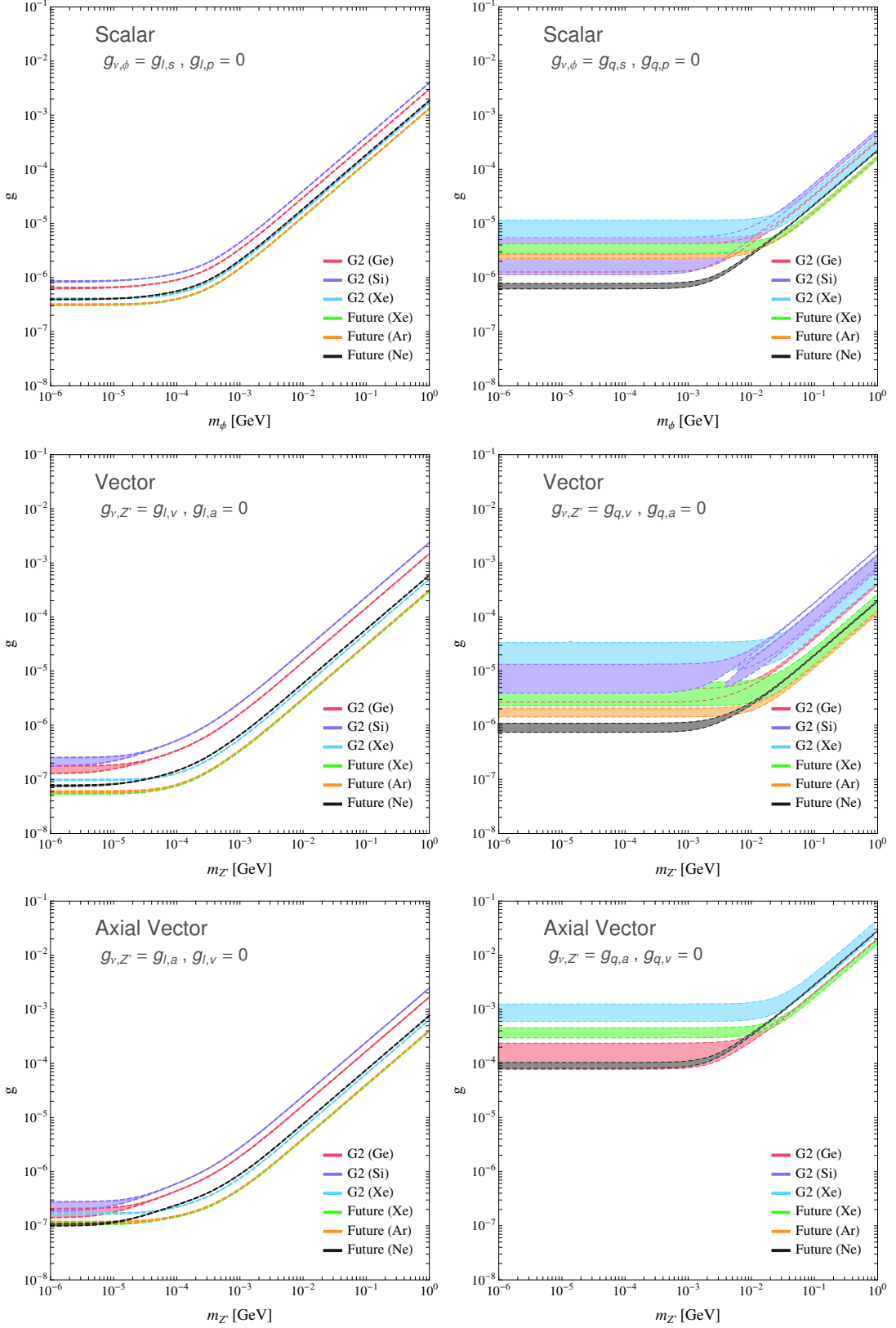
FIG. 4. Electron recoil (left) and nuclear recoil (right) 90% CL limits for a variety of target materials, using natural isotopic abundances. Top: scalar coupling; middle row: vector coupling; lower panels: axial vector coupling. The thickness of the bands represent the difference between the nominal (least constraining) and optimistic (most constraining) threshold configurations of Tab. I.
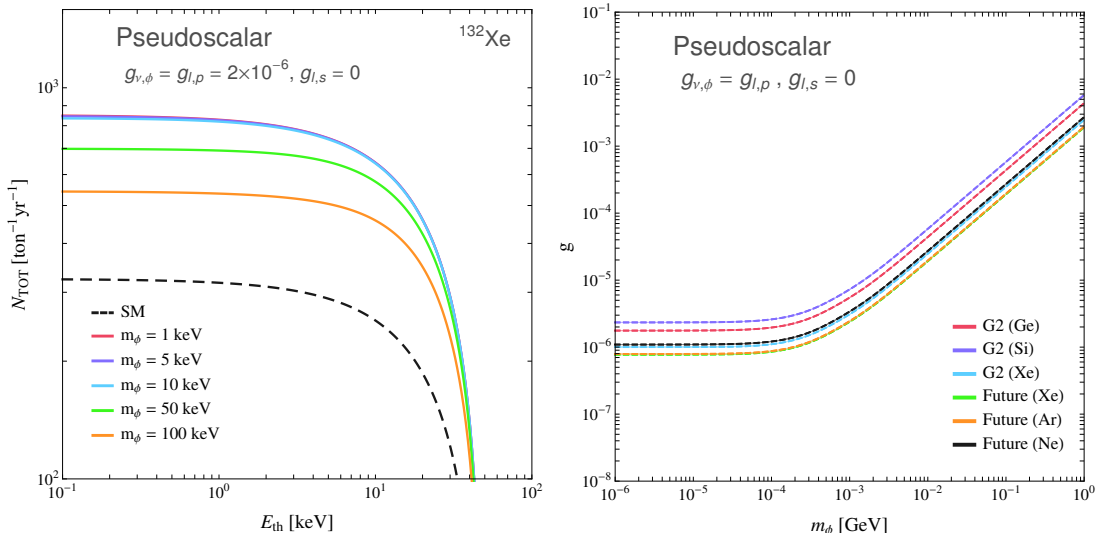
FIG. 5. Electron recoil integrated rates (left) and sensitivity (right) for a pseudoscalar coupling.

vanishing couplings to bottom quarks.

- **Coupling to quarks only**
  The "SN1987A" region (Supernova 1987A losing half of its energy via Z' emission) is sensitive to couplings to nucleons.

- **Any coupling**
  Fifth force searches (tests of gravitational, Casimir and van der Waals forces) would be sensitive to all scenarios, except if the couplings to protons, neutrons and electrons are proportional to the electric charge, in such a way that the test bodies used in these experiments are essentially neutral under the new interaction.

Finally, we present an estimate of the current bounds based on available data from the Super-CDMS Soudan results [62], CDMSlite [63], and the latest LUX data [64]. For SuperCDMS we take an exposure of 577 kg days, and an energy range $E_{th} = 1.6$ keV, $E_{max} = 10$ keV. We neglect detector resolution effects, and use the efficiency presented in Figure 1 of Ref. [62]. We take the 11 candidate events of this study as background. In the case of LUX, the exposure was 38.4 kg years, with an energy range $E_R = [1.1, 25]$ keV. We take the efficiency from Figure 1 of Ref. [64]. To model the detector resolution, we adopt a Gaussian smearing of E_R, with a width $\sigma_{E_R}/\text{keV} \simeq 0.2(E_R/\text{keV})^{0.6}$ [65].[7] The small gap in the LUX region corresponds to the coupling range in which the interference between the new mediator and the Z boson suppresses the expected event rate.

In the case of CDMSlite, we analysed separately electron and nuclear recoils separately. The exposure of its second run [63] was 70 kg days, with a threshold as low as $E_R = 0.056$ keV for electron recoils ($E_R \sim 150$ eV for nuclear recoils). We consider the efficiency, energy bands and background (we assume a flat background) defined in Fig. 3 and Table I of Ref. [63]. We have derived independent constraints on nuclear recoils (solid brown line) and electron recoils (dashed brown line), since CDMSlite cannot distinguish between these. In this case spectral information is available as the data are split into four energy bins, and we modify the likelihood ratio analysis accordingly.

The current and future bounds presented here make it clear that, in the case where a new mediator couples only to baryons or charged leptons, DD experiments actually lead to the strongest constraints for large regions of the parameter space. In the case of lepton-only coupling, the strong electron recoil limits push into the $\sim$ MeV mediator window, inaccessible to fixed target experiments, and can strengthen limits by a factor of ~ 5 for mediators above ~ 100 MeV. If the new mediator couples more strongly to light quarks than to electrons, nuclear bounds from DD experiments dominate the parameter space, as the light grey and pink regions of Fig. 6 cease to apply. In fact, the limits that we have derived in this paper from current results of LUX, SuperCDMS, and CDMSlite represent the strongest bounds on this scenario to date.[8]

---

[7] This can be inferred via the relationship $E_R = 13.7\,\text{eV} \cdot (n_e + n_\gamma)$, where n_e and n_γ are the measured electron and photon numbers, and the error on these quantities as a function of energy is shown in Figure 12 of [65].

[8] Although having a larger $\nu - q$ scattering than $\nu - e$ may seem unnatural, a simple example of a gauge invariant theory with this property would be a broken $B - 3L_3$ gauge symmetry with a light mediator.
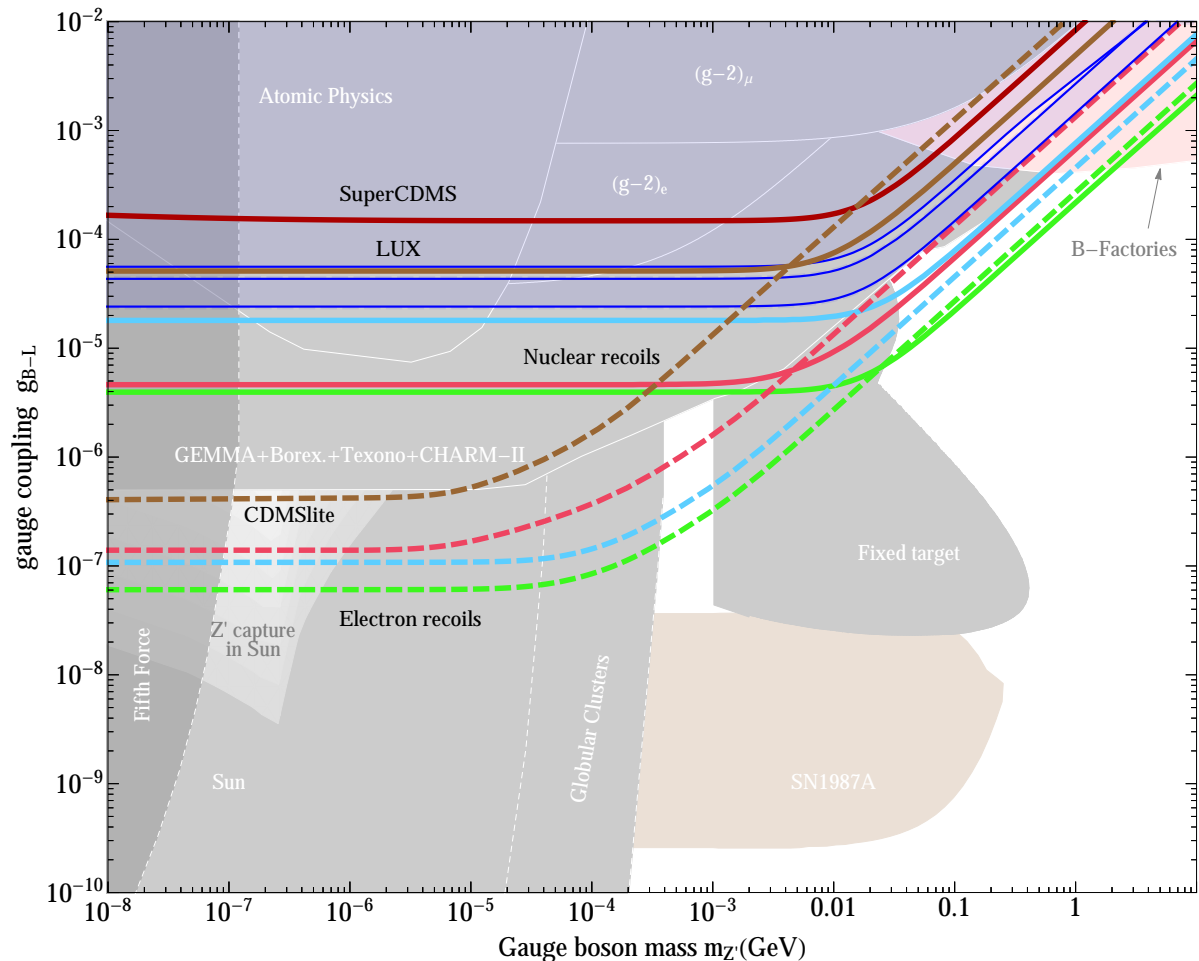
FIG. 6. Projected 90% CL constraints on the B-L model for nuclear recoils (solid lines) and electron recoils (dashed) in the optimistic scenarios for G2 germanium (red), G2 xenon (blue) and future xenon (green). We also show approximate bounds derived from the current SuperCDMS (red line), CDMSlite (brown solid and dashed lines), and LUX data (blue shaded region). The gap in the region bounded by LUX is due to destructive interference between the new mediator and the standard model contribution. Our bounds are overlaid on existing constraints. To translate these bounds to the other possible scenarios, one should keep in mind that some bounds (intermediate grey) only apply when the new mediator couples to leptons. The supernova bound (brown) only applies to couplings to baryons, while B-factory bounds (pink) require both. The fifth force constraint (dark grey) applies in either case. The grey regions, the neutrino scattering bound and the pink pregion, and the supernova limits are respectively taken from Refs. [57], [58], and [59].

VI. CONCLUSIONS

In this work we have investigated the potential of direct detection (DD) dark matter experiments to use the flux of solar neutrinos to improve our understanding of particle physics and of the Sun, as well as to probe the existence of hypothetical new messenger particles.

The observation of neutrino-electron scattering in next generation DD experiments would lead to an independent measurement of $\sin^2\theta_W$ at unprecedented low energies which cannot be reached by dedicated experiments. A 4.5% precision can be obtained in this measurement from next-generation (G2) experiments, and hypothetical future Xe and Ar experiments could reduce this down to 1.4%. Future dedicated neutrino ex-

periments such as HyperKamiokande and JUNO [40] will further constrain the solar neutrino flux normalizations, allowing an even more precise DD-inferred measurement of $\sin^2\theta_W$.

Data from future DD experiments will also help constrain measurements of solar parameters. Most notably, the total pp neutrino flux could be measured up to 0.6% precision (compared with the current experimental precision of approximately 10%, and a projected percent-level precision from SNO+ [66]). Other observables related to the solar composition – namely the opacity and metallicity – could also be improved, albeit with the help of complementary probes.

Crucially, these forecasts are for setups very similar to DD experiments that will become operational and begin data taking over the next few

years. In contrast, planned dedicated neutrino experiments are still up to a decade away.

We have studied the conditions under which DD experiments can be sensitive to solar neutrinos from the CNO cycle. We observed that this would require a light target, combined with an extremely low energy threshold and good discrimination between electron and nuclear recoils. Due to the small atomic mass of Ne, gaseous TPCs of this material with an energy threshold of approximately 0.1 keV could be ideal (although no discrimination NR/ER has yet been achieved at such low energies).

Finally, we have studied the contributions from new physics to neutrino interactions, concentrating on simplified models designed to include the effects of light mediators (scalar, pseudoscalar, vector, and axial vector) which couple to neutrinos and either quarks or electrons. Figures 4 and 5 show constraints that can be placed on such new particles based on future experiments. Through the specific example of a $B - L$ gauge boson, we have shown in Fig. 6 that direct detection experiments are already competitive with bounds from other origins.

Existing bounds from other works rely heavily on a new boson coupled to neutrinos and charged leptons.

However, we have shown that a coupling of a new boson to neutrino and quarks is already constrained by both SuperCDMS and LUX.

Electron recoil measurements can furthermore explore regions of the parameter space hitherto inaccessible to other searches, such as the gap below $m_\phi = 2m_e$ between fixed target and stellar bounds.

The expected event rate from coherent neutrino scattering in the next generations of dark matter direct detection experiments is often presented as a nearly impenetrable barrier to the search for new physics. Apart from being the first signal of coherent neutrino scattering, we have demonstrated here that DD experiments' sensitivity to the solar neutrino fluxes presents manifold scientific opportunities, both in terms of precision measurements and for the exploration of new physics, well beyond the original scope of these instruments.

ACKNOWLEDGMENTS

[1] B. Cabrera, L. M. Krauss, and F. Wilczek, Phys. Rev. Lett. **55**, 25 (1985).

[2] A. K. Drukier, K. Freese, and D. N. Spergel, Phys. Rev. **D33**, 3495 (1986).

[3] J. Monroe and P. Fisher, Phys. Rev. **D76**, 033007 (2007), arXiv:0706.3019 [astro-ph].

[4] J. D. Vergados and H. Ejiri, Nucl. Phys. **B804**, 144 (2008), arXiv:0805.2583 [hep-ph].

[5] L. E. Strigari, New J. Phys. **11**, 105011 (2009), arXiv:0903.3630 [astro-ph.CO].

[6] A. Gutlein et al., Astropart. Phys. **34**, 90 (2010), arXiv:1003.5530 [hep-ph].

[7] J. Billard, L. Strigari, and E. Figueroa-Feliciano, Phys.Rev. **D89**, 023524 (2014), arXiv:1307.5458 [hep-ph].

[8] J. H. Davis, JCAP **1503**, 012 (2015), arXiv:1412.1475 [hep-ph].

[9] F. Ruppin, J. Billard, E. Figueroa-Feliciano, and L. Strigari, Phys.Rev. **D90**, 083510 (2014), arXiv:1408.3581 [hep-ph].

[10] P. Grothaus, M. Fairbairn, and J. Monroe, Phys.Rev. **D90**, 055018 (2014), arXiv:1406.5047 [hep-ph].

[11] C. A. J. O'Hare, A. M. Green, J. Billard, E. Figueroa-Feliciano, and L. E. Strigari, Phys. Rev. **D92**, 063518 (2015), arXiv:1505.08061 [astro-ph.CO].

[12] J. B. Dent, B. Dutta, J. L. Newstead, and L. E. Strigari, (2016), arXiv:1602.05300 [hep-ph].

[13] P. L. Brink (SuperCDMS), J. Low. Temp. Phys. **167**, 1093 (2012).

[14] D. S. Akerib et al. (LZ), (2015), arXiv:1509.02910 [physics.ins-det].

[15] H. Davoudiasl, H.-S. Lee, and W. J. Marciano, Phys. Rev. **D89**, 095006 (2014), arXiv:1402.3620 [hep-ph].

[16] S. Vagnozzi, K. Freese, and T. H. Zurbuchen, (2016), arXiv:1603.05960 [astro-ph.SR].

[17] A. Serenelli, P. Scott, F. L. Villante, A. C. Vincent, M. Asplund, S. Basu, N. Grevesse, and C. Pena-Garay, (2016), arXiv:1604.05318 [astro-ph.SR].

[18] L. Baudis, A. Ferella, A. Kish, A. Manalaysay, T. Marrodan Undagoitia, et al., JCAP **1401**, 044 (2014), arXiv:1309.7024 [physics.ins-det].

[19] B. Collaboration, Nature **512**, 383 (2014).

[20] J. Billard, L. Strigari, and E. Figueroa-Feliciano, Phys.Rev. **D91**, 095023 (2015), arXiv:1409.0050 [astro-ph.CO].

[21] M. Schumann, L. Baudis, L. Btikofer, A. Kish, and M. Selvi, (2015), arXiv:1506.08309 [physics.ins-det].

[22] C. Peña Garay and A. Serenelli, (2008), arXiv:0811.2424 [astro-ph].

[23] W. Haxton and A. Serenelli, (2009), arXiv:0902.0036 [astro-ph.SR].

[24] W. C. Haxton, R. G. Hamish Robertson, and A. M. Serenelli, ARA&A **51**, 21 (2013), arXiv:1208.5723 [astro-ph.SR].

[25] A. Serenelli, C. Peña Garay, and W. Haxton, Phys.Rev. **D87**, 043001 (2013), arXiv:1211.6740 [astro-ph.SR].

[26] K. Olive et al. (Particle Data Group), Chin.Phys. **C38**, 090001 (2014).

[27] H. J. Behrend et al. (CELLO), Phys. Lett. **B183**, 400 (1987).

[28] J. Erler and M. J. Ramsey-Musolf, Phys.Rev. **D72**, 073003 (2005), arXiv:hep-ph/0409169 [hep-ph].

[29] C. Bouchiat and C. A. Piketty, *11th International Symposium on Lepton and Photon Interactions at High Energies Ithaca, New York, August 4-9, 1983*, Phys. Lett. **B128**, 73 (1983).

[30] S. G. Porsev, K. Beloy, and A. Derevianko, Phys. Rev. Lett. **102**, 181601 (2009), arXiv:0902.0335 [hep-ph].

[31] C. Boehm, Phys.Rev. **D70**, 055007 (2004), arXiv:hep-ph/0405240 [hep-ph].

[32] B. Batell, D. McKeen, and M. Pospelov, Phys. Rev. Lett. **107**, 011803 (2011), arXiv:1103.0721 [hep-ph].

[33] C. Boehm, T. A. Ensslin, and J. Silk, J. Phys. **G30**, 279 (2004), arXiv:astro-ph/0208458 [astro-ph].

[34] R. H. Helm, Phys. Rev. **104**, 1466 (1956).

[35] G. Duda, A. Kemper, and P. Gondolo, JCAP **0704**, 012 (2007), arXiv:hep-ph/0608035 [hep-ph].

[36] E. Aprile et al., Phys. Rev. D **83**, 082001 (2011), arXiv:1101.3866 [astro-ph.IM].

[37] L. E. Strigari, (2016), arXiv:1604.00729 [astro-ph.CO].

[38] M. C. Gonzalez-Garcia, M. Maltoni, and T. Schwetz, JHEP **11**, 052 (2014), arXiv:1409.5439 [hep-ph].

[39] J. Bergstrom, M. C. Gonzalez-Garcia, M. Maltoni, and T. Schwetz, JHEP **09**, 200 (2015), arXiv:1507.04366 [hep-ph].

[40] F. An et al. (JUNO), J. Phys. **G43**, 030401 (2016), arXiv:1507.05613 [physics.ins-det].

[41] J. Bergstrom, M. C. Gonzalez-Garcia, M. Maltoni, C. Pena-Garay, A. M. Serenelli, and N. Song, JHEP **03**, 132 (2016), arXiv:1601.00972 [hep-ph].

[42] J. Mammei (MOLLER), Nuovo Cim. **C035N04**, 203 (2012), arXiv:1208.1260 [hep-ex].

[43] K. Abe et al., (2011), arXiv:1109.3262 [hep-ex].

[44] K. Abe et al. (Super-Kamiokande), Phys. Rev. **D83**, 052010 (2011), arXiv:1010.0118 [hep-ex].

[45] F. L. Villante, ApJ **724**, 98 (2010), arXiv:1006.3875 [astro-ph.SR].

[46] J. N. Bahcall and A. M. Serenelli, ApJ **626**, 530 (2005), astro-ph/0412096.

[47] J. N. Bahcall, Phys. Rev. **C65**, 025801 (2002), arXiv:hep-ph/0108148 [hep-ph].

[48] M. Asplund, N. Grevesse, A. J. Sauval, and P. Scott, ARA&A **47**, 481 (2009), arXiv:0909.0948 [astro-ph.SR].

[49] C. Amole et al. (PICO), Submitted to: Phys. Rev. D (2016), arXiv:1601.03729 [astro-ph.CO].

[50] C. Bobin et al., *Proceedings of the 5th International Workshop, TAUP'97, Gran Sasso, Italy, September 7-11, 1997*, Nucl. Phys. Proc. Suppl. **70**, 90 (1999).

[51] F. J. Iguaz et al., (2015), arXiv:1512.01455 [physics.ins-det].

[52] I. G. Irastorza et al., JCAP **1601**, 034 (2016), arXiv:1512.06294 [physics.ins-det].

[53] M. Cirelli, E. Del Nobile, and P. Panci, JCAP **1310**, 019 (2013), arXiv:1307.5955 [hep-ph].

[54] R. J. Hill and M. P. Solon, Phys. Rev. **D91**, 043505 (2015), arXiv:1409.8290 [hep-ph].

[55] J. M. Alarcon, J. Martin Camalich, and J. A. Oller, Phys. Rev. **D85**, 051503 (2012), arXiv:1110.3797 [hep-ph].

[56] J. M. Alarcon, L. S. Geng, J. Martin Camalich, and J. A. Oller, Phys. Lett. **B730**, 342 (2014), arXiv:1209.2870 [hep-ph].

[57] R. Harnik, J. Kopp, and P. A. Machado, JCAP **1207**, 026 (2012), arXiv:1202.6073 [hep-ph].

[58] S. Bilmis, I. Turan, T. M. Aliev, M. Deniz, L. Singh, and H. T. Wong, Phys. Rev. **D92**, 033009 (2015), arXiv:1502.07763 [hep-ph].

[59] E. Rrapaj and S. Reddy, (2015), arXiv:1511.09136 [nucl-th].

[60] A. I. Studenikin, in *Proceedings, Les Rencontres de Physique de la Vallee d'Aoste, La Thuile, Italy, March 1 - 7, 1998* (1998) arXiv:hep-ph/9808219 [hep-ph].

[61] F. Jegerlehner and A. Nyffeler, Phys. Rept. **477**, 1 (2009), arXiv:0902.3360 [hep-ph].

[62] R. Agnese et al. (SuperCDMS), Phys. Rev. Lett. **112**, 241302 (2014), arXiv:1402.7137 [hep-ex].

[63] R. Agnese et al. (SuperCDMS), Phys. Rev. Lett. **116**, 071301 (2016), arXiv:1509.02448 [astro-ph.CO].

[64] D. S. Akerib et al. (LUX), (2015), arXiv:1512.03506 [astro-ph.CO].

[65] D. S. Akerib et al. (LUX), (2015), arXiv:1512.03133 [physics.ins-det].

[66] S. Andringa et al. (SNO+), Adv. High Energy Phys. **2016**, 6194250 (2015), arXiv:1508.05759 [physics.ins-det].